Above 600 mV Open Circuit Voltage BiI_3 Solar Cells

*Devendra Tiwari[a], Dominic Alibhai[b], and David J Fermin[a,]**

[a]School of Chemistry, University of Bristol, Bristol – BS8 1TS, UK

[b]Wolfson Bioimaging Facility, Faculty of Biomedical Sciences, University of Bristol, University Walk, Bristol BS8 1TD, UK

*david.fermin@bristol.ac.uk

ABSTRACT

Phase-pure BiI_3 films obtained by a versatile gas phase iodination of Bi_2S_3 are investigated as an absorber in photovoltaic devices. This preparation method leads to highly crystalline BiI_3 films featuring rhombohedral phase and a high-degree of stacking order. The films are composed of micrometer-sized flat grains distributed homogenously across the F:doped SnO_2 (FTO) substrate exhibiting an indirect band gap transition at 1.72 eV. High-level calculations based on G_0W_0 approximation are used to rationalize the electronic structure of BiI_3, confirming the band gap value estimated experimentally. The films show p-type conductivity with an acceptor density of the order of 10^{15} cm^{-3}. Solar cells with the architecture Glass/FTO/TiO_2/BiI_3/F8/Au, where F8 is Poly(9,9-di-n-octylfluorenyl-2,7-diyl), display record open-circuit voltage above 600 mV and overall power conversion efficiency of 1.2% under AM 1.5G illumination. The large open-circuit potential is rationalized in terms of carrier lifetimes longer than 1 ns as probed by time-resolved photoluminescence spectroscopy.

TOC GRAPHICS

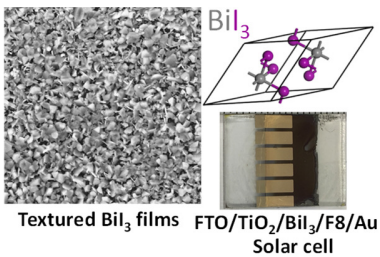

Sustainable photovoltaic technologies beyond Si solar cells represent huge opportunities in key areas such as large-scale building integration and competitive tandem technologies close to 30%.[1,2] This strategy requires new solar absorbers based on Earth-abundant materials which can offer different alternatives to existing CdTe and $CuInGa(S,Se)_2$ (CIGS) technologies.[3–6] Hybrid perovskite solar cells have experienced an unprecedented rise from basic science to a technology close to commercialization, particularly in the context of Si-tandem solar cells, although significant challenges remain in terms of stability.[7] $Cu_2ZnSn(S,Se)_4$ has been the key target in the context of Earth-abundant CIGS replacement, however, efficiency remains hindered by loss-mechanism yet to be fully elucidated.[8–10] These developments have led to the establishment of guiding principles for the design of solar absorbers based on the concept of "defect tolerant materials", with Bi being one of the elements in these strategies.[5,6] Indeed, Bi^{3+} and Pb^{2+} are heavy and highly polarizable cations associated with large spin-orbit coupling effects, dielectric constants, and band dispersion, resulting in low recombination probabilities and better charge separation.[5,6,11] Bi compounds such as methylammonium bismuth iodide, bismuth chalcohalides, bismuth sulphide, silver bismuth sulphide and bismuth iodide, have been tested as solar absorbers with power conversion efficiencies up to 6.3%.[12–19] Previously, we reported on $BiFeO_3$ all oxide-solar cells with a record power-conversion efficiency of 4%.[18] BiI_3 is particularly attractive as a binary compound composed of low-cost elements and suitable optoelectronic properties.[20]

BiI_3 fundamental optical transitions have been reported in the range of 1.67 to 1.90 eV, featuring capture cross-sections larger than 10^5 cm^{-1} for energies above 2 eV.[20–23] Additionally, minority carrier lifetime (τ_h) and electron mobilities (μ_e) of 1.54 ns and 250 $cm^2\,V^{-1}\,s^{-1}$ have been reported in BiI_3 single crystals.[20,24,25] The current record efficiency of BiI_3 thin-film cells was reported by

Hamdeh and co-workers, with a V_{OC} value below 400 mV and a power conversion efficiency of approximately 1%, although no statistical analysis of these performance indicators was reported.[17] In contrast to single crystals, thin films deposited either by solution or physical vapor deposition are characterized by a shorter τ_h (250 ps), which could be a limiting factor in PV performance.[20] In this work, we develop a new methodology for preparing high-quality rhombohedral BiI_3 thin-films based on gas-phase iodination of Bi_2S_3. The films exhibit a high degree stacking order with τ_h values longer than 1 ns as estimated from time-resolved photoluminescence spectroscopy. PV devices with the architecture: Glass/FTO/TiO_2/BiI_3/F8/Au, where F8 is Poly(9,9-di-n-octylfluorenyl-2,7-diyl), display record open-circuit voltage above 600 mV and overall efficiency of 1.2% under AM 1.5 illumination. Electronic and vibrational fingerprints of the phase-pure BiI_3 films are rationalized based on calculations employing G_0W_0 approximation and Density Functional Perturbation Theory.

BiI_3 films are prepared by a sequential method starting from spin coating a $Bi(NO_3)_3$ and thiourea precursor solution onto FTO, followed by thermolysis at 200 ^oC to produce a homogenous Bi_2S_3 film which is subsequently iodinated upon exposure to the I_2 gas. This methodology is inspired in our previous report on the fabrication of PbI_2 photocathodes,[26] although in this case the Bi_2S_3 is placed above the I_2 granules which are heated to 200 ^oC (see **supporting information S3** for further details). The reaction is governed by Pearson's hard soft acid base principle in which the polarizable Bi^{+3} (soft-acid) spontaneously exchanges a hard S^{-2} base partner with a polarizable I^- (soft-base).[27]

The structure, morphology and phase purity of the as-grown BiI_3 films are investigated by X-ray diffraction and Raman spectroscopy (**Figure 1**). XRD of the film on the FTO substrate (**Figure 1a**) reveals crystallization of BiI_3 in its common rhombohedral structure (R-3, space group: 148). No peaks due to sulphide, oxide, and oxy-iodide are detected. The high intensity of (003) peak at ~12^o suggests high-degree of orientation along the c-axis of the unit cell. The Bi atom is octahedrally coordinated to I atoms forming hexagonally-close-packed layers interacting by weak Van der Waal force along c-axis with the Bi atom, effectively occupying one-third of octahedral sites.[28] The SEM image in **Figure 1b** is characterized by flake-shaped grains with sizes in the range of 700 to 1200 nm homogenously distributed across the substrate. This growth behavior is similar to that observed for PbI_2 films.[26]

Figure 1c displays the Raman spectrum of BiI_3, showing three distinctive bands assigned to A_g and E_g modes. These assignments are supported by theoretically calculated spectra using density functional perturbation theory as shown in **Figure 1d** (full spectrum is plotted in **Figure s1**). The measured and calculated spectra exhibit a remarkable similarity in the range of 80 to 160 cm^{-1}. The spectral information below 83 cm^{-1} cannot be accessed in our spectrometer. The modes at 98 and 113 cm^{-1} are LO phonon modes at the Γ and Z special points, respectively. The nature of three vibrational modes at 98, 114 and 126 cm^{-1} is captured in the movies provided in **supporting information S1 and S2**.

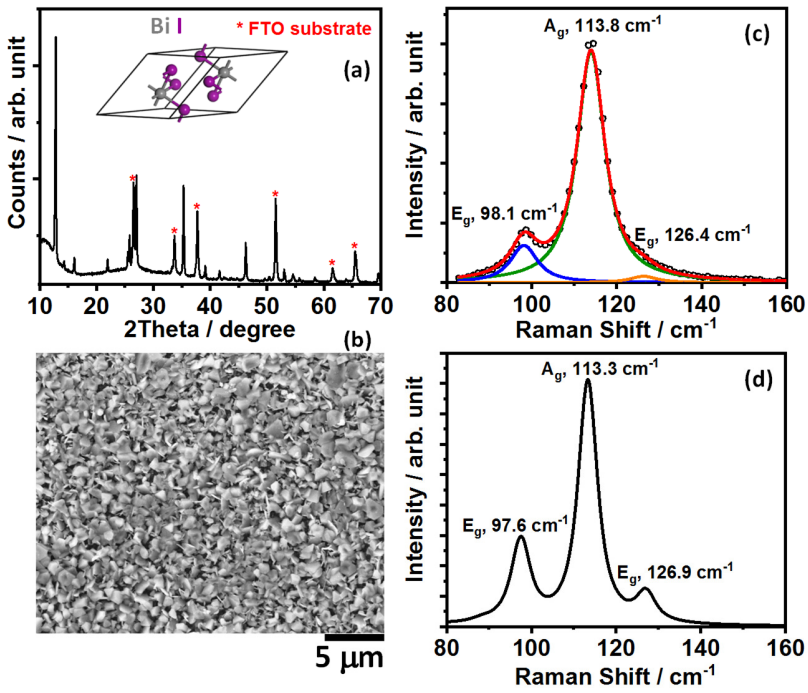

Figure 1: Structural and morphological characterization of BiI_3 thin films: X-ray diffraction with an inset depicting the BiI_3 unit cell (a), top-view scanning electron micrograph (b), measured Raman spectrum under 785 nm laser excitation (c) and calculated Raman spectrum employing density functional perturbation theory (d).

Figure 2a displays the optical transmittance and reflectance spectra of 230 nm thick BiI_3 films on the FTO coated glass substrates, showing a sharp absorption behavior between 650 to 700 nm. Considering an indirect band gap transition, a value of 1.72 can be estimated from the Tauc's plot in **Figure 2b.** As mentioned previously, there is some debate in the literature concerning the value of the indirect band gap transition which ranges between 1.65 to 1.90 eV, with reports of direct transitions between 1.8 and 2 eV.[20–23] The dispersion in the reported experimental and computed value of E_g has been found to depend on experimental methodology and computational

level.[16,20,22,23,29–33] The most detailed optical study has been reported by Podraza et al., showing an indirect transition at 1.67 eV,[22] which is close to our findings. On the other hand, hybrid HSE functional DFT by Lehner et al. estimated a value of 1.93 eV.[16]

Figures 2c and **2d** summarize our estimations of the electronic structure of BiI_3 employing quasiparticle G_0W_0 approximation showing that the lowest energy transition has an indirect nature with a value of 1.68 eV. Komatsu and Kaifu established that the temperature dependence of the BiI_3 band gap has a gradient of -3.7 x 10^{-4} eV/K between 286 and 77 K, and -1.8 x 10^{-4} eV/K between 77 and 6 K.[34] Based on these findings, the calculated band gap is expected to decrease to approximately 1.59 eV at room temperature. It is important to highlight that G_0W_0 calculations consistently underestimated experimental band gap values by 200 meV on average in over 200 materials.[35,36] Consequently, the difference in our computed value and the experimental band gap on our thin films (**Figure 2b**) and on single crystals by Podraza et al.[22] can be considered within the error of the method.

Although G_0W_0 calculations provide accurate accounts of spin-orbit coupling, band dispersions, and width, this comes at the expense of high computational costs which limit calculating the projected density of states. However, this information is available with a good level of accuracy from the elegant work by Lehner et al. employing DFT with hybrid functionals.[16] The conduction band is formed of highly covalent I 5p and Bi 6p hybridized states split due to spin-orbit coupling, while the valence band is primarily composed of I 5p orbital with a minor contribution from Bi 6s electrons. Calculations also show that the conduction band is much more dispersed than the

valence band as a result of spin-orbit coupling promoted by Bi^{+3} ion. This results in a lighter effective mass of electrons in comparison to holes, thus higher electron mobility. This observation is also consistent with experimental studies on BiI_3 single crystals, showing effective electron mass five times lower than holes and electron mobility up to 250 $cm^2\ V^{-1}\ s^{-1}$.[25] The high covalent interaction in the conduction band is also responsible for a substantial in-plane Born effective charge of 5.43. These optoelectronic features are very attractive in the context of thin-film PV devices.

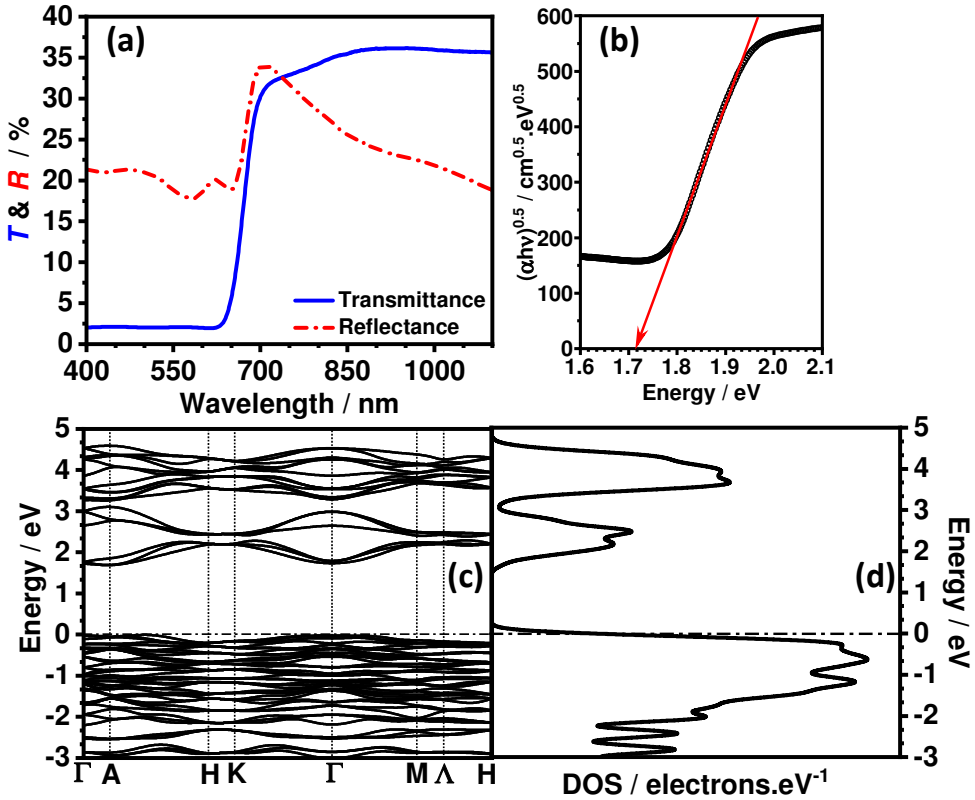

Figure 2: Transmittance and reflectance spectrum of BiI_3 thin films (a), Tauc's plot showing an indirect transition at 1.72 eV (b), band structure (c) and density of states (DOS) (d) of BiI_3 calculated employing quasiparticle G_0W_0 approximation.

Electrochemical impedance spectroscopy in non-aqueous electrolyte solutions was employed to estimate the doping density of the films. Analysis based on the Mott-Schottky plot in **Figure s2** confirmed the p-type nature of BiI_3 with estimates of the majority carrier density in the range of 2.8×10^{15} to 1.4×10^{16} cm^{-3}, considering the contrast in relative permittivity between in-plane ($\varepsilon_{//} = 8.6$) and out-of-plane ($\varepsilon_{\perp} = 54$).[37] These values should be considered as an upper limit as the effective roughness of the material is not considered in the calculations. PbI_2 films obtained by a similar route were also characterized by a low doping density.[26] The analysis also shows that the flat band potential (E_{fb}) is located at 1.53 V vs SHE, placing the valence band maxima (VBM) at approximately 5.97 eV with respect to the vacuum level, which is close to values obtained from photoemission spectroscopy.[16] Considering E_g = 1.72 eV, the conduction band minima (CBM) is set close to 4.25 eV.

Current-voltage characteristics of 10 devices featuring an active area of 4 mm^2 under AM1.5 G (100 mW cm^{-2}) illumination are shown in **Figure 3a**. Devices were designed with an architecture Glass/FTO/TiO_2/BiI_3/F8/Au, with a BiI_3 film thickness of 230 nm. As described in the **supporting information S3**, electron (TiO_2) and hole (F8) transporting layers were processed by spin-coating. The best performing device displayed a power conversion efficiency (η) of 1.21 % with short-circuit current (J_{SC}), fill-factor (FF) and open-circuit voltage (V_{OC}) of 5.28 mA/cm^2, 37.6%, and 607 mV, respectively. These figures of merits represent a clear improvement over the state-of-the-art, in particular, the 200 mV increase in V_{OC}.[17] The external quantum efficiency (EQE) for the champion cell show a maximum value close to 35% as displayed in **Figure 3b**. The variation of

the key figure of merits was less than 10%, illustrating the reproducibility in the preparation method.

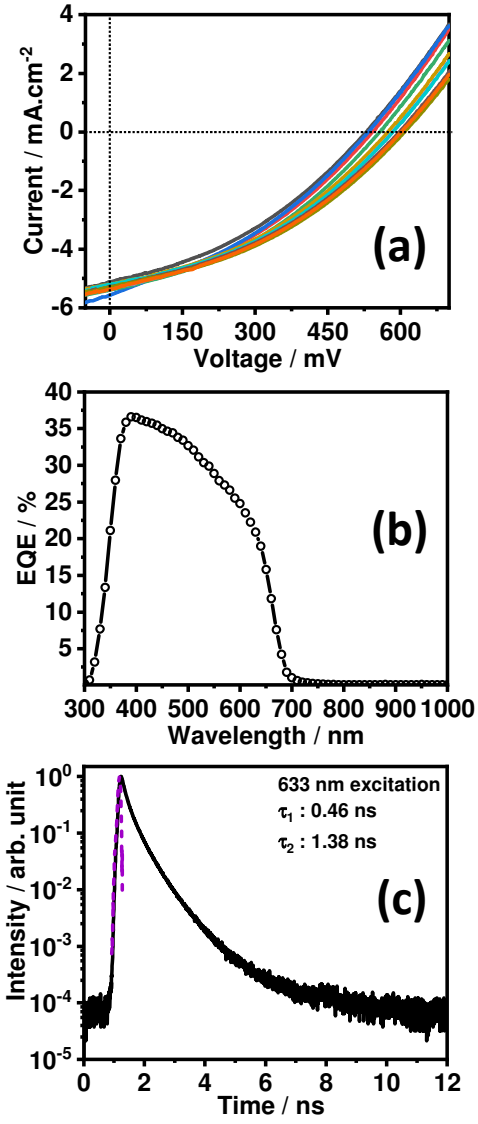

Figure 3: PV performance of glass/FTO/TiO_2/BiI_3/F8/Au devices: *J-V* characteristics of 10 cells under AM1.5G (100 mW/cm^2) illumination (a) and characteristic external quantum efficiency spectrum (b). Time-resolved photoluminescence spectrum of the BiI_3 films (c). The purple trace corresponds to the instrument response function (IRF).

The improved device performance with respect to previous reports can be linked to device architecture and the quality of the BiI_3 film. Conducting polymers such as poly-triarylamine (PTAA; IP = 5.1 eV) and poly-indacenodithiophene-difluorobenzo-thiadiazole (PIDT-DFBT; IP = 5.5 eV) has been employed as hole transport layer (HTL) by Lehner et al.[16] The HTL with higher IP resulted in an improvement of V_{OC} from 220 mV to 420 mV, but at a cost of short-circuit current (J_{SC}), leading to only an incremental change in overall η from 0.3 to 0.32 %.[16] Hamdeh et al. used a thin layer of V_2O_5 which resulted in J_{SC} of up to 8 mA cm^{-2} and η of 1.0 %, however, the V_{OC} remained limited to 365 mV.[17] The use of F8 in our devices is inspired by Ganose et al. theoretical studies on BiSI, suggesting that high IP value (5.8 eV) of this polymer offers a better match to the VBM.[38] This point partially accounts for the record V_{OC} values measured in our devices. Indeed, we have investigated cells employing F8 as HTL but following previous protocols in which commercially available BiI_3 powder are spin-coated to the TiO_2 surface (so-called "direct" method).[20] The corresponding *J-V* curves (**Figure s3a**) exhibited J_{SC} and FF 10 to 15 % lower values, while the V_{OC} drops by 56 % in comparison to the devices prepared by our gas phase iodination method. The EQE spectra also show significantly lower values at wavelengths close to the band edge for the devices prepared via the direct method (**Figure s3b**). This results strongly suggest that the minority carrier lifetime is significantly different in these two films.

Finally, **Figure 3c** shows a characteristic time-resolved photoluminescence measurement of BiI_3 prepared by gas phase iodination. The data were fitted to a biexponential function, yielding two lifetimes values of around 460 ps and 1.4 ns. These values are comparable to the lifetimes

measured on BiI_3 single crystals and significantly longer than in thin-films reported in previous studies.[17,20] It is rather difficult to quantitatively rationalize the increase in V_{OC} with carrier lifetime as there is no theoretical framework directly combining these two parameters. Repins and co-workers provided an empirical correlation after analyzing a large number of CIGS devices, showing that V_{OC} is strongly dependent of carrier lifetime in the range below 10 ns.[39] Consequently, the high quality of the BiI3 thin films generated by our method is key for achieving record V_{OC} and PCE values. There is significant room for improvement in device architecture, not only in terms of better alignment of ETL and HTL layers to the absorber layer but also in the carrier collection efficiencies. Indeed, it is anticipated that interfacial recombination at the boundaries with carrier extracting layers is the main performance limiting factors in these devices.

Supporting Information

Movies illustrating the Raman vibrational modes, BiI_3 thin film deposition and cell fabrication, film characterization and device measurements, computational detail, BiI_3 Raman spectrum calculated by DFPT, Mott-Schottky plot of the BiI_3 film in dichloromethane, device performance of cells fabricated by direct spin-coating of BiI_3 particles

Notes

The authors declare no competing financial interest.

Acknowledgments

DT and DJF both are grateful to the UK Engineering and Physical Sciences Research Council, EPSRC) the PVTEAM grant (EP/L017792/1). DJF also thanks the support received through the Institute of Advanced Studies of the University of Bristol, (University Research Fellowship 2015). Electron microscopy and impedance spectroscopy are performed using the instrumentation funded by EPSRC Capital grant (EP/ K035746/1). Authors also acknowledge Wolfson Bioimaging Facility at the University of Bristol for fluorescence lifetime imaging microscope (FLIM) procured through BBSRC/EPSRC-funded Synthetic Biology Research Centre grant: L01386X. Computational work is facilitated by the supercomputing facilities at the Advanced Computing Research Centre, the University of Bristol (www.bris.ac.uk/acrc/). All the data presented in this paper can be freely accessed from the Bristol's Research Data Repository (data.bris.ac.uk/data).

References

(1) Sofia, S. E.; Mailoa, J. P.; Weiss, D. N.; Stanbery, B. J.; Buonassisi, T.; Peters, I. M. Economic Viability of Thin-Film Tandem Solar Modules in the United States. *Nat. Energy* **2018**, *3*, 387–394.

(2) Ballif, C.; Lufkin, S.; Rey, E. Integrated Thinking for Photovoltaics in Buildings. *Nat. Energy* **2018**, *3*, 438–442.

(3) Haegel, N. M.; Margolis, R.; Buonassisi, T.; Feldman, D.; Froitzheim, A.; Garabedian, R.; Green, M.; Glunz, S.; Henning, H. M.; Holder, B.; et al. Terawatt-

Scale Photovoltaics: Trajectories and Challenges. *Science* **2017**, *356*, 141–143.

(4) Peter, L. M. Towards Sustainable Photovoltaics: The Search for New Materials. *Philos. Trans. R. Soc. A Math. Phys. Eng. Sci.* **2011**, *369*, 1840–1856.

(5) Ganose, A. M.; Savory, C. N.; Scanlon, D. O. Beyond Methylammonium Lead Iodide: Prospects for the Emergent Field of Ns^2 Containing Solar Absorbers. *Chem. Commun.* **2017**, *53*, 20–44.

(6) Brandt, R. E.; Stevanović, V.; Ginley, D. S.; Buonassisi, T. Identifying Defect-Tolerant Semiconductors with High Minority-Carrier Lifetimes: Beyond Hybrid Lead Halide Perovskites. *MRS Commun.* **2015**, *5*, 265–275.

(7) Snaith, H. J. Present Status and Future Prospects of Perovskite Photovoltaics. *Nat. Mater.* **2018**, *17*, 372–376.

(8) Wallace, S. K.; Mitzi, D. B.; Walsh, A. The Steady Rise of Kesterite Solar Cells. *ACS Energy Lett.* **2017**, *2*, 776–779.

(9) Tiwari, D.; Skidchenko, E.; Bowers, J.; Yakushev, M. V.; Martin, R.; Fermin, D. J. Spectroscopic and Electrical Signatures of Acceptor States in Solution-Processed $Cu_2ZnSn(S,Se)_4$ Solar Cells. *J. Mater. Chem. C* **2017**, *5*, 12720–12727.

(10) Bourdais, S.; Chone, C.; Delatouche, B.; Jacob, A.; Larramona, G.; Moisan, C.; Lafond, A.; Donatini, F.; Rey, G.; Siebentritt, S.; et al. Is the Cu/Zn Disorder the Main Culprit for the Voltage Deficit in Kesterite Solar Cells? *Adv. Energy Mater.* **2016**, *6*, 1502276-1–21.

(11) Lee, L. C.; Huq, T. N.; MacManus-Driscoll, J. L.; Hoye, R. L. Z. Research Update:

Bismuth-Based Perovskite-Inspired Photovoltaic Materials. *APL Mater.* **2018**, *6*, 084502-1–16.

(12) Cao, Y.; Bernechea, M.; Maclachlan, A.; Zardetto, V.; Creatore, M.; Haque, S. A.; Konstantatos, G. Solution Processed Bismuth Sulfide Nanowire Array Core/Silver Sulfide Shell Solar Cells. *Chem. Mater.* **2015**, *27*, 3700–3706.

(13) Hahn, N. T.; Self, J. L.; Mullins, C. B. BiSI Micro-Rod Thin Films: Efficient Solar Absorber Electrodes? *J. Phys. Chem. Lett.* **2012**, *3*, 1571–1576.

(14) Bernechea, M.; Miller, N. C.; Xercavins, G.; So, D.; Stavrinadis, A.; Konstantatos, G. Solution-Processed Solar Cells Based on Environmentally Friendly $AgBiS_2$ Nanocrystals. *Nat. Photonics* **2016**, *10*, 521–525.

(15) Park, B. W.; Philippe, B.; Zhang, X.; Rensmo, H.; Boschloo, G.; Johansson, E. M. J. Bismuth Based Hybrid Perovskites $A_3Bi_2I_9$ (A: Methylammonium or Cesium) for Solar Cell Application. *Adv. Mater.* **2015**, *27*, 6806–6813.

(16) Lehner, A. J.; Wang, H.; Fabini, D. H.; Liman, C. D.; Hébert, C.-A.; Perry, E. E.; Wang, M.; Bazan, G. C.; Chabinyc, M. L.; Seshadri, R. Electronic Structure and Photovoltaic Application of BiI_3. *Appl. Phys. Lett.* **2015**, *107*, 131109-1–4.

(17) Hamdeh, U. H.; Nelson, R. D.; Ryan, B. J.; Bhattacharjee, U.; Petrich, J. W.; Panthani, M. G. Solution-Processed BiI_3 Thin Films for Photovoltaic Applications: Improved Carrier Collection via Solvent Annealing. *Chem. Mater.* **2016**, *28*, 6567–6574.

(18) Tiwari, D.; Fermin, D. J.; Chaudhuri, T. K.; Ray, A. Solution Processed Bismuth

Ferrite Thin Films for All-Oxide Solar Photovoltaics. *J. Phys. Chem. C* **2015**, *119*, 5872–5877.

(19) Hoye, R. L. Z.; Lee, L. C.; Kurchin, R. C.; Huq, T. N.; Zhang, K. H. L.; Sponseller, M.; Nienhaus, L.; Brandt, R. E.; Jean, J.; Polizzotti, J. A.; et al. Strongly Enhanced Photovoltaic Performance and Defect Physics of Air-Stable Bismuth Oxyiodide (BiOI). *Adv. Mater.* **2017**, *29*, 1702176-1–10.

(20) Brandt, R. E.; Kurchin, R. C.; Hoye, R. L. Z.; Poindexter, J. R.; Wilson, M. W. B.; Sulekar, S.; Lenahan, F.; Yen, P. X. T.; Stevanovic, V.; Nino, J. C.; et al. Investigation of Bismuth Triiodide (BiI_3) for Photovoltaic Applications. *J. Phys. Chem. Lett.* **2015**, *6*, 4297–4302.

(21) Watanabe, K.; Karasawa, T.; Komatsu, T.; Kaifu, Y. Optical Properties of Extrinsic Two-Dimensional Excitons in BiI_3 Single Crystals. *J. Phys. Soc. Japan* **1986**, *55*, 897–907.

(22) Podraza, N. J.; Qiu, W.; Hinojosa, B. B.; Xu, H.; Motyka, M. A.; Phillpot, S. R.; Baciak, J. E.; Trolier-Mckinstry, S.; Nino, J. C. Band Gap and Structure of Single Crystal BiI_3: Resolving Discrepancies in Literature. *J. Appl. Phys.* **2013**, *114*, 033110-1–8.

(23) Jellison, G. E.; Ramey, J. O.; Boatner, L. A. Optical Functions of BiI_3 as Measured by Generalized Ellipsometry. *Phys. Rev. B - Condens. Matter Mater. Phys.* **1999**, *59*, 9718–9721.

(24) Dmitriyev, Y. N.; Bennett, P. R.; Cirignano, L. J.; Klugerman, M. B.; Shah, K. S. Bismuth Iodide Crystals as a Detector Material: Some Optical and Electrical

Properties. *SPIE Conf. Hard X-Ray, Gamma-Ray, Neutron Detect. Phys.* **1999**, *3768*, 521–529.

(25) Lintereur, A. T.; Qiu, W.; Nino, J. C.; Baciak, J. Characterization of Bismuth Tri-Iodide Single Crystals for Wide Band-Gap Semiconductor Radiation Detectors. *Nucl. Instruments Methods Phys. Res. Sect. A Accel. Spectrometers, Detect. Assoc. Equip.* **2011**, *652*, 166–169.

(26) Tiwari, D.; Fermin, D. J. Textured PbI_2 Photocathodes Obtained by Gas Phase Anion Replacement. *Electrochim. Acta* **2017**, *254*, 223–229.

(27) Drago, R. S. On Pearson's Quantitative Statement of HSAB. *Inorg. Chem.* **1973**, *12*, 2211–2212.

(28) Zobel, J.; Trotter, T. The Crystal Structure of SbI_3 and BiI_3. *Zeitschrift für Krist.* **1966**, *123*, 67–72.

(29) Sun, X. X.; Li, Y. L.; Zhong, G. H.; Lü, H. P.; Zeng, Z. The Structural, Elastic and Electronic Properties of BiI_3: First-Principles Calculations. *Phys. B Condens. Matter* **2012**, *407*, 735–739.

(30) Schulter, M.; Cohen, M. L.; Kohn, E.; Fon, Y. Electronic Structure of BiI_3. *Phys. Status Solidi* **1976**, *78*, 737–747.

(31) Yorikawa, H.; Muramatsu, S. Theoretical Study of Crystal and Electronic Structures of BiI_3. *J. Phys. Condens. Matter* **2008**, *20*, 325220-1–7.

(32) Kaifu, Y.; Komatsu, T. Optical Properties of Bismuth Tri-Iodide Single Crystals. II. Intrinsic Absorption Edge. *J. Phys. Soc. Japan* **1976**, *40*, 1377–1382.

(33) Zhang, W.-B.; Xiang, L.-J.; Li, H.-B. Theoretical Perspective of Energy Harvesting Properties of Atomically Thin BiI_3. *J. Mater. Chem. A* **2016**, *4*, 19086–19094.

(34) Komatsu, T.; Kaifu, Y. Optical Properties of Bismuth Tri-Iodide Single Crystals. I Interband Transitions. *J. Phys. Soc. Jpn.* **1976**, *40*, 1062–1068.

(35) Van Schilfgaarde, M.; Kotani, T.; Faleev, S. Quasiparticle Self-Consistent GW Theory. *Phys. Rev. Lett.* **2006**, *96*, 226402-1–4.

(36) Hautier, G.; Miglio, A.; Ceder, G.; Rignanese, G. M.; Gonze, X. Identification and Design Principles of Low Hole Effective Mass P-Type Transparent Conducting Oxides. *Nat. Commun.* **2013**, *4*, 2292-1–7.

(37) Du, M. H.; Singh, D. J. Enhanced Born Charges in III-VII, IV-VII_2, and V-VII_3 Compounds. *Phys. Rev. B - Condens. Matter Mater. Phys.* **2010**, *82*, 045203-1–5.

(38) Ganose, A. M.; Butler, K. T.; Walsh, A.; Scanlon, D. O. Relativistic Electronic Structure and Band Alignment of BiSI and BiSeI: Candidate Photovoltaic Materials. *J. Mater. Chem. A* **2016**, *4*, 2060–2068.

(39) Repins, I. L.; Metzger, W. K.; Perkins, C. L.; Li, J. V.; Contreras, M. A. Correlation between Measured Minority-Carrier Lifetime and C(In,Ga)Se_2 device Performance. *IEEE Trans. Electron Devices* **2010**, *57*, 2957–2963.